Submitted to *Ironmaking and Steelmaking*, October ??? 2006

Interaction between Molten Steel and Runner Materials during Steel Ingot Bottom Teeming Process

Prof. Lifeng Zhang (**correspondence author**)
Department of Materials Science and Engineering
Norwegian University of Science and Technology (NTNU)
Høgskoleringen 8,
7491 Trondheim, Norway.
Tel: 0047-73594123 Fax: 0047-73550203
Email: lifeng.zhang@material.ntnu.no

Prof. Brian G. Thomas
Department of Mechanical & Industrial Engineering
University of Illinois at Urbana-Champaign
1206 W. Green St., Urbana
IL 61801, USA
Tel: 1-217-333-6919 Fax: 1-217-244-6534
Email: bgthomas@uiuc.edu

Ken Eakin
Ellwood Quality Steel Company
700 Moravia St., New Castle, PA 16101
Email: KEAKIN@elwd.com

Abstract

Inclusions in industrial-cast bottom-teemed ingots and runners of plain carbon steel are investigated using ultrasonic detection, optical microscope observation, and SEM analysis. The composition, size distribution, entrapment locations, and sources of ingot inclusions were revealed by examining all the macro-inclusions (larger than 20μm) that were observed in 35,000 mm^2 of sample surface area. Based on 78 non-sulfide inclusions observed, around 3.23×10^7 macro-inclusions per m^3 steel exist in the ingot, with a size distribution increasing with decreasing size. Inclusions are distributed uniformly within a given horizontal section through the ingot, but with more found towards the bottom. The largest inclusions exceed 7mm and originated from mold flux in the ingot. The largest inclusion source appears to be reoxidation, as evidenced by 59% of the ingot inclusions composed of pure alumina clusters and lumps. Eroded refractories from the ladle well block and ladle inner nozzle bricks accounted for 31% of the ingot inclusions. Reaction between the high-Mn steel, reoxidation with air, and reaction with silica in the runner bricks caused very large (>7mm) compound inclusions of SiO_2-MnO-Al_2O_3 in the center of runners.

Key words: Steel Ingot, Inclusions, Runner, Mold flux, MnO-riched Inclusions, Exogenous Inclusions

1. Introduction and Methodology

Non-metallic inclusions are a significant problem in cast steels that can lead to problems in castings that require expensive casting repairs or rejection. The mechanical properties of steel are controlled to a large degree by the volume fraction, size, distribution, composition and morphology of inclusions and precipitates, which act as stress raisers. Through with decreasing percentage compared with continuous casting, ingot casting is still important because some low-alloy steel grades and steel for special applications can only be produced by this process. These include high carbon chromium bearing steel, [1] thick plate, seamless tube, forgings, bars and wire rods.[2]

The authors did an extensive investigation on large inclusions in the bottom-teemed ingot of 1022 carbon steel[3], including inclusion number density, size distribution, composition, location in the ingot, and their sources. However, the reason for high MnO (MnO ~10%) inclusions, well found in ingot, is still not well explained. The current paper focuses on this topic.

2. Process Description and Methodology

The ingot production process of this bottom-teemed ingot of 1022 carbon steel (with composition in Table 1) includes the following steps:

- Scrap melting by an ultra high powered eccentric bottom tapping electric arc furnace.
- Alloying during tapping process
- Ladle refining for heating, alloying and induction stirring
- Vacuum degassing to remove hydrogen
- Ladle calcium treatment
- Ingot bottom teeming

The teeming process delivers the steel down a trumpet, through a “spider” distributing the flow into 7-8 round-section runners with inner diameter of 50.8mm, across and up through inlets with the same diameter into each mold in a cluster of 7-8 ingots. The compositions of the mold flux and refractories are shown in Table 2 and Figure 1, including the ladle lining, well block, filler sand, trumpet, and runner bricks. The ingots in this study were round with 0.33m diameter, 4.70m height and 2.91 metric tonnes in weight. The total filling rate was around 1.4 tonne/min (23kg/s), with 3.3kg/s to each ingot. This increased the ingot level at 4.87mm/s. The typical filling time was 13-18 minutes.

After final solidification, the ingot was sectioned and sampled for inclusion analysis. The solidified runner bar/spider for this ingot was also examined. After polishing, the samples were first observed under an optical microscope to mark the locations of all inclusions larger than 20μm in diameter. Then, the detailed morphology and composition of each inclusion was analyzed by scanning electron microscope (SEM) using Energy Dispersive X-Ray Analysis. Runner materials samples after teeming process are collected, polished, and observed under SEM.

2. Ingot Inclusions Analysis

As reported in our another paper [3], for non-sulfide > 20μm inclusions, 59% were pure alumina or alumina/FeO inclusions, which are believed to arise mainly from air reoxidation; 22% were from ladle well block refractory; 9% from the ladle inner nozzle; 8% from mold flux and runner bricks, and 2% from slag inclusions (not mold flux). Example inclusion from runner brick is shown in Figure 1. Inclusions from runner brick materials have the following characteristics:

- Irregular shape
- Large size (over several hundred μm)
- Hign MnO content (will discussed later)

While, inclusions from mold flux, should have the following characteristics:

- being in liquid state under molten steel temperature, thus should be spherical shape or filling in the space between steel dendrite arms, as shown in Figure 3
- with high Na_2O and K_2O content
- low MnO content

So the inclusion in Fig.2 should be from runner brick but not from mold flux.

3. Runner Lining Observations

The used runner bricks, shown in figure 4, were also investigated. A layer of black slag-like material was observed between the runner steel and the surrounding refractory brick that partly adhered to both surfaces. The shape of the steel in the round runners was flattened across the top, presumably due to the combined effects of solidification shrinkage and gravity. The slag layer built up more in this top region of the runner, where it averages ~3mm thick and was 0.3mm thick at the bottom (figure 5). Evidence of the molten steel breaking through cracks in the runner brick and leaking around the bricks is observed as large attached fins in several places (Fig.4). The black slag layer contains gas porosity. Analysis using SEM detection shows that three layers exist in the used brick near the steel: original brick, intermediate layer and reaction layer (runner slag) (Fig.5). The composition of three layers is shown in Table 3. From the original brick to the reaction layer, the SiO_2 concentration decreases, while the levels of other oxides, including Al_2O_3 and MnO generally increase.

4. Inclusions in Runner Steel Samples

Samples of steel in the runners were taken near the upgate (sample R1), half-way along the runner (sample R2), and near the trumpet (sample R3), as shown in figure 6. The runner steel samples were cut into 4 quadrants and observed under optical microscope for inclusions larger than 20µm, which were further analyzed by SEM.

4.1. Large central inclusions

Extremely huge inclusions (near upgate, runner midpoint) and large voids (near trumpet) were observed in the center of many of the runner samples. They have the following characteristics:

- Large size, exceeding 7mm in size, such as shown in Fig. 6.
- The matrix of the large inclusions contains ~18%Al_2O_3, ~40%SiO_2, ~40%MnO (surface average). While there are many needle-shaped inclusions of pure Al_2O_3, around 5-10µm in diameter, and 10-100µm in length.
- Distributed along the steel dendritic boundaries.

The morphology and composition of these big inclusions are shown in figure 7. In the matrix of the large inclusions, different spots have slightly different compositions. The light crystalline phase is the needle-shaped pure Al_2O_3. These pure Al_2O_3 needles likely crystallized inside the large central inclusions while they were still liquid. These inclusions are entrained runner slag.

Slag inclusions remain in a liquid state while the steel solidifies. Thus, they can be pushed by the growing dendrite tips, to coagulate and collect at the last place to freeze near the runner center, where macroporosity (voids) are also common. The closeup views of the inclusion boundaries in Fig. 7 clearly show that slag filled in the interdendritic porosity. This filling was incomplete, as indicated by the interdendritic porosity remaining in Figure 8. This figure clearly reveals the dendritic tip shape around the interior of the void.

Although they were found in many runner samples, inclusions rich in MnO were rarely found in the ingot. This suggests that these inclusions require long times for reactions to occur, such as between the liquid steel and the refractories. Thus, they likely form later during teeming, and are more likely to remain in the runner.

4.2. Other inclusions

In addition to the large central inclusion, many pure alumina clusters (> 20μm) were observed throughout the section of runner steel samples. The pure alumina inclusions are also well observed in ingot steel samples, as discussed in our paper [3]. The sources of these pure alumina inclusions can only be deoxidation by Al, or reoxidation by air absorption.

However, steel deoxidation is executed during tapping, from which to steel refining, vacuum degassing, teeming and to final solidification of the ingot it takes long time, even more than 1 hour. Thus, big size alumina clusters from deoxidation have enough time to be removed by flow transport in ladles and ingot. They also have enough opportunity to attach other inclusions with different composition during motion in ladles, trumpet and ingot, which changes them not to be pure alumina. Thus, the observed pure alumina inclusions are more likely from reoxidation by air absorption, and form later during teeming, such as at the end period of teeming. The current trail did not use argon shrouding between ladle and trumpet during teeming, thus the air absorption should be very serious.

It should be emphasized that when reoxidation from air absorption occurs during casting of molten steel containing [Al], [Si], and [Mn], the dissolved aluminum [Al] is more easily reoxidized than [Si] and [Mn]. After [Al] is locally depleted, FeO, MnO, SiO_2 may form [4], but they will be reduced by [Al] diffusing from surrounding places in the bulk. [4]

In addition to alumina clusters, there were also many sulfide inclusions and single compound inclusions with high MnO content. Figure 9 shows one of these high-MnO inclusions. These single inclusions do not distribute along the dendrite boundary, and contain more SiO_2 than the inclusions in Fig.7 and 8. They may be entrained late and not in liquid state, or no enough time to be pushed to the center of the runner.

The number of inclusions observed in each quadrant is included in figure 10. The inclusions generally show a random distribution between quadrants of the samples near the runner ends, where the flow conditions are complicated. In the mid-length sample, more inclusions are found in the upper half of the runner. This is likely due to the stable fully-developed pipe flow conditions allowing the lower-density inclusions to drift upwards and redistribute at this location.

4.3. Source of Runner Slag and associated Inclusions

These results suggest that two different reactions caused the black runner slag, composition gradients in the lining, and the resulting inclusions containing SiO_2, MnO, and Al_2O_3: (1) re-oxidation of the steel and (2) Mn reduction of SiO_2 in the brick.

The increase of Al_2O_3 near the runner surface (Table 3) indicates that either prior air exposure caused alumina particles that attached to the wall, or that silica in the lining refractory reacted with dissolved Al according to:

$$(SiO_2)+[Al]\rightarrow(Al_2O_3)+[Si] \tag{1}$$

Secondly, Mn dissolved in the liquid steel has concentrated onto the refractory surface and reduced some of the silica in the brick to Si according to the follow reaction:

$$(SiO_2)+[Mn]\rightarrow(MnO)+[Si] \tag{2}$$

This well-known reaction occurs after the dissolved Al is locally depleted. It increases as the Mn level in the steel increases. [5-7] The second source of the high MnO in the runner slag layer is from prior air entrainment and reoxidation of steel. The many pure alumina clusters are found in the ingot steel samples, prove that this did occur. If air absorption was high enough, then the oxygen remaining after reacting with dissolved Al can then react with Mn to form MnO. This MnO may deposit on the lining surface, or contribute to MnO inclusions directly.

The reaction (slag surface) layer is easily eroded and entrained into the steel for two reasons. Firstly, the refractory structure is weakened by the reaction. Secondly, at the temperature of liquid steel, the reaction products may be in a liquid state. Thus, inclusion material may easily become entrained into the flowing molten steel to be captured by the solidifying front as defects in the final product.

The gas porosity in the black runner slag is likely caused by CO bubbles produced from the following reaction between carbon in the steel with SiO_2 in the brick [6]

$$(SiO_2)+[C]\rightarrow CO\uparrow+[Si] \quad (3)$$

The above findings explain how runner slag forms from air absorption and interaction between high-Mn molten steel and runner bricks that contain SiO_2. To avoid the quality problems that likely result from this runner slag, it is recommended that SiO_2 in all of the refractories be avoided, by increasing the Al_2O_3 content up to 60%, or by using ZrO_2-based refractories. A comprehensive refractory-lining specification is essential for the production of high quality forging ingots. Consistent acceptable composition, porosity, bulk density and strength of the bricks should be maintained, in order to control inclusion content of the final product.

Reduction of MnO by carbon may also occurs (Eq.4). But the main components of the runner lining refractory are SiO_2 and Al_2O_3, thus reaction (3) firstly happen. When more and more MnO builds up, then reaction (4) may take place.

$$(MnO)+[C]\rightarrow CO\uparrow+[Mn] \quad (4)$$

The reason that the slag layer built up more in this top region of the runner are possibly 1). Due to the gravitational force and solidification shrinkage, the shape of the steel in the round runners was flattened across the top (as shown in Fig.6), thus there is more space at the top between the runner steel and the lining refractory; 2) When the slag is still liquid state, due to the generation of CO bubbles (Eq.3), more slags float to the top of the runner and adhere the inner wall.

5. Summary and Conclusions

- A comprehensive investigation of inclusions in industrial bottom-teemed ingots and runners of plain carbon steel was undertaken using ultrasonic detection, optical microscope observation, and SEM analysis. The composition, size distribution, entrapment locations, and sources of ingot inclusions were revealed from the inclusions larger than 20µm that were observed.
- Reaction between the high-Mn steel, reoxidation with air, and reaction with silica in the runner bricks caused very large (>7mm) compound inclusions of SiO_2-MnO-Al_2O_3 in the runner center.
- Ingot quality can be improved only by careful control of teeming to prevent air reoxidation, and by maintaining high control of the lining refractories. Silica-containing bricks should be avoided.

Acknowledgements:

This work was supported by a grant from the Ingot Metallurgy Forum, which is gratefully acknowledged. Thanks are also extended to Elwood Quality Castings for conducting the industrial trials, and to Danielle Q. Baird at Timken, Inc. for help with planning. Microscopy was performed using the facilities at the Center for Microanalysis of Materials at the University of Illinois, which is partially supported by the U.S. Department of Energy under grant DEFG02-91-ER45439. Finally, thanks are owed to Jim Mabon and to the Machine Shop at the Department of Mechanical & Industrial Engineering for help with sample preparation.

References:

1. E. Fuchs and P. Jonsson, "Inclusion Characteristic in Bearing Steel Before and During Ingot Casting," High Temperature Materials and Processes, Vol. 19 (5), 2000, 333-343.
2. K. Sumitomo, M. Hashio, T. Kishida, A. Kawami, "Bottom Pouring and Ingot Quality at Sumitomo Metal Industries," Iron and Steel Engineer, Vol. 62 (3), 1985, 54-61.
3. L. Zhang, B. Rietow, K. Eakin, B.G. Thomas, "Large Inclusions in Plain-Carbon Steel Ingots Cast by Bottom Teeming," ISIJ Inter., Vol. 46 (5), 2006, 670-679.
4. Y. Habu, H. Kitaoka, Y. Yoshii, T. Emi, Y. Iida, T. Ueda, "Origin and Remival of Large Non-metallic Inclusions Present during Continuous Casting of Wide Slabs," Tetsu-To-Hagane, Vol. 62 (14), 1976, 1803-1812.
5. S.M. Kim, L. W-K, P.S. Nicholson, A.E. Hamielec, "Corrosion of Alumina-Silicate Refractories in Fe-Mn Alloys," American Ceramic Society Bulletin, Vol. 53 (7), 1974, 543-547.
6. N. Reitsema and P.W. Wright, "The Decomposition of Silicate Refractories in Contact with Molten Steel," 1st International Conference on Refractories, (Tokyo, Japan), 1983, 795-810.
7. A. Muan, "Physical Chemistry of Electric Furnace Refractories," Electric Furnace Steelmaking Conference Proceedings, ISS, USA, Vol. 43, 1985, 384-388.

Captions:

Table 1 Steel composition in the trial

Table 2 Composition of flux and linings used at ladle, trumpet, runner and ingot mold

Table 3 Sources of >20μm inclusions in ingot

Fig.1 Schematic of bottom teeming process

Fig.2 Inclusions from mold flux and runner brick

Fig.3 Used Runner Brick

Fig.4 Runner slag

Fig.5 Runner steel samples (near upgate, runner midpoint, and near trumpet from left to right)

Fig.6 MnO-rich inclusions at the center of runner steel samples

Fig.7 MnO-rich inclusions distribute along the dendritic gap

Fig.8 MnO-rich inclusions near the edge of runner steel samples

Fig.9 Inclusion distribution on runner steel samples

Table 1 Steel composition in the trial

Elements	[C]	[P]	[S]	[Al]	[Si]	[Mn]	[Ni]	[Cr]	[Mo]	[Cu]
%	.22	.011	.014	.029	.26	1.01	.09	.11	.02	.17

Table 2 Composition of flux and linings used at ladle, trumpet, runner and ingot mold

	Ladle Lining						Nozzle Sand	Trumpet & Runner		Mold Flux
	Wall	Bottom	Well block	Inner Nozzle	Slide gates	Collector Nozzle		Brick	Filler	
SiO_2	0-5	0.8	0.10	1.00	0.5	10-13	27.6	50.8	0.9	29.0-36.0
Al_2O_3	0-5	0.5	91.22	94.00		83-87	11.8	44.5	0.8	15.0-21.0
MgO	80-100	40.1	6.01	Trace	97.0		7.1	0.1	37.7	<2.0
CaO		57.6	2.51	Trace	1.8		0	0.1	55.6	1.0-5.0
Fe_2O_3	0.5	0.9	0.03		0.2	1-2	18.6	1.0	4.2	5.0-11.0
Na_2O			<0.02	0.20		<1		0.47		4.0-6.0
K_2O										<2.0
TiO_2			0.02			1-3		2.1		<1.5
ZrO_2				2.50			0			
Cr_2O_3							32.9			
MnO										<1.0
F										<0.5
C_{total}	5-15						0.6			23.0-26.0

Table 3 Composition of the used runner brick and runner slag

	Original brick		Intermediate layer	Reaction layer (runner slag)
	Analysis 1	Analysis 2		
SiO_2	59.15	52.49	27.11	17.99
Al_2O_3	34.79	45.04	68.63	52.56
MnO	0.01	0.00	1.15	20.01
Na_2O	0.14	0.66	1.46	1.73
K_2O	1.69	1.30	1.20	1.22
TiO_2	2.25	0.20	0.25	1.72
Fe_2O_3	1.97	0.31	0.20	4.77

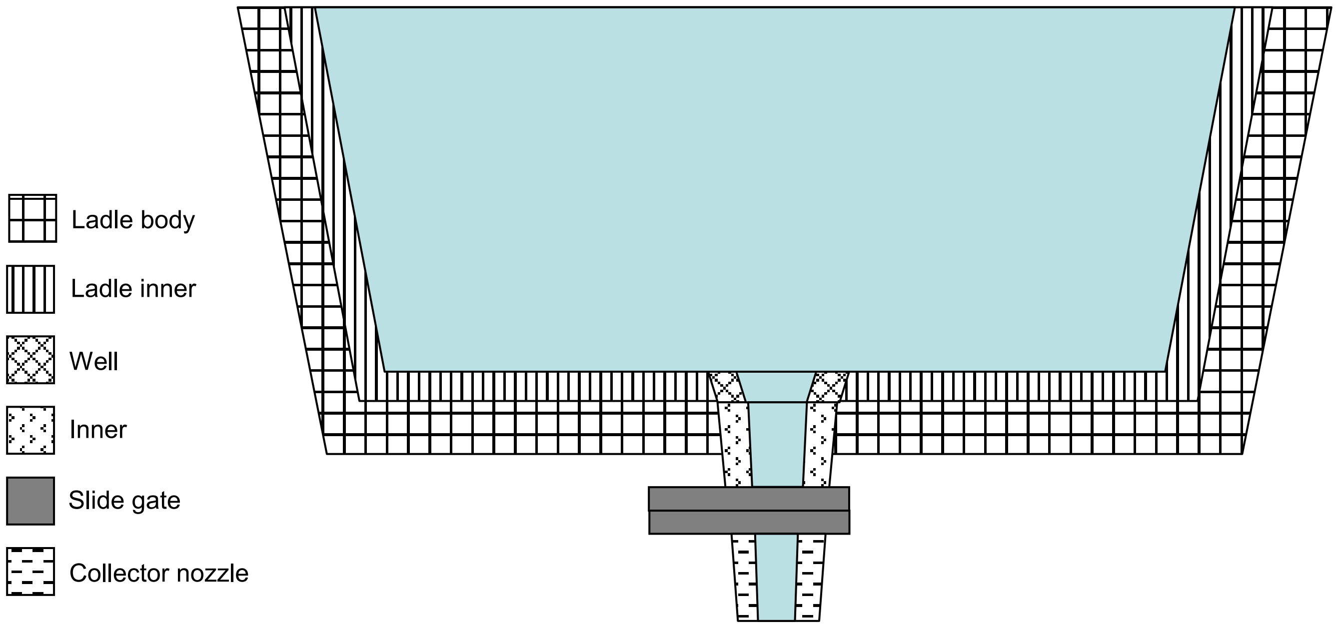

(a) Ladle lining materials

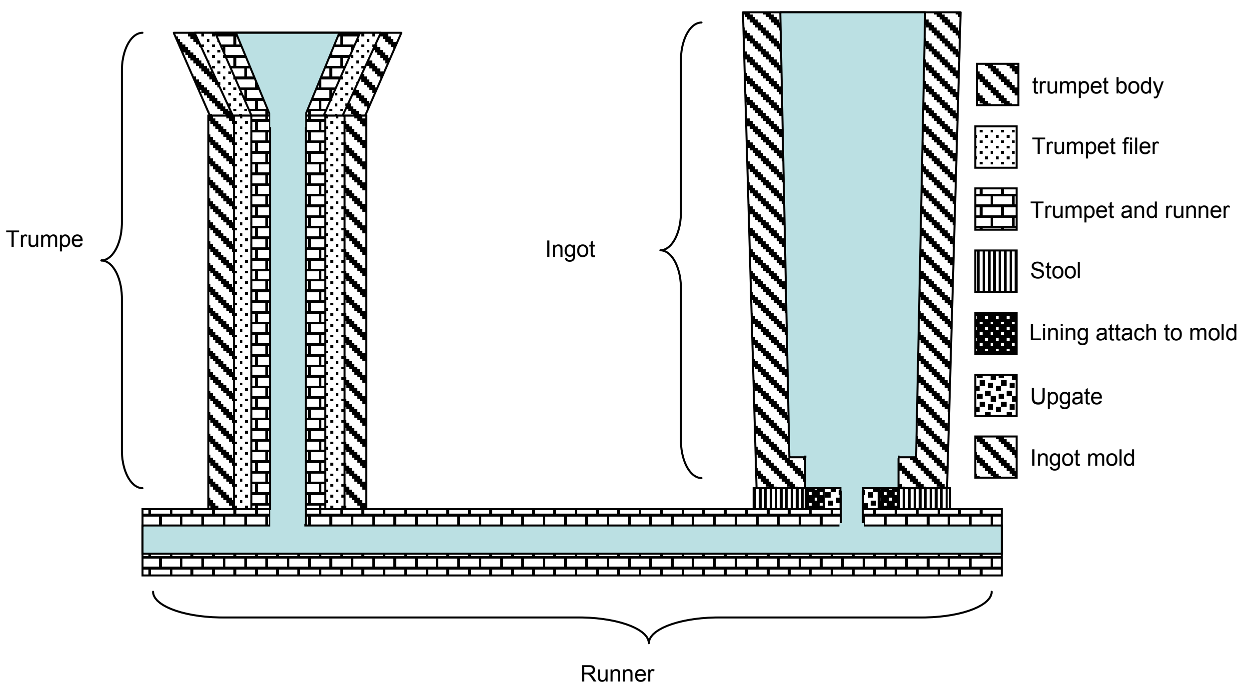

(b) Trumpet, runner and ingot mold

Fig.1 Schematic of bottom teeming process

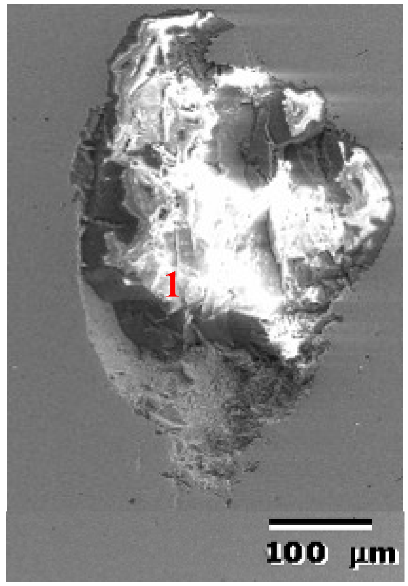

Al_2O_3 22.05%, SiO_2 47.02%, MgO 1.88%, CaO 3.15%, FeO 8.51%, MnO 11.95%, K_2O 1.52%, Na_2O 5.07%

Fig.2 Inclusions from runner brick

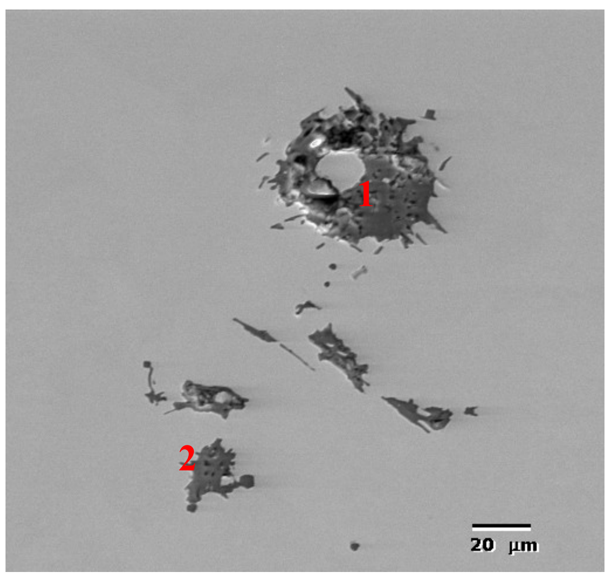

1: Al_2O_3 83.22, MgO 4.36, K_2O 10.26 CaO 2.16

2: Al_2O_3 81.05, MgO 3.62, K_2O 10.27, CaO 1.04, FeO 4.03

Fig.3 Inclusions from mold flux

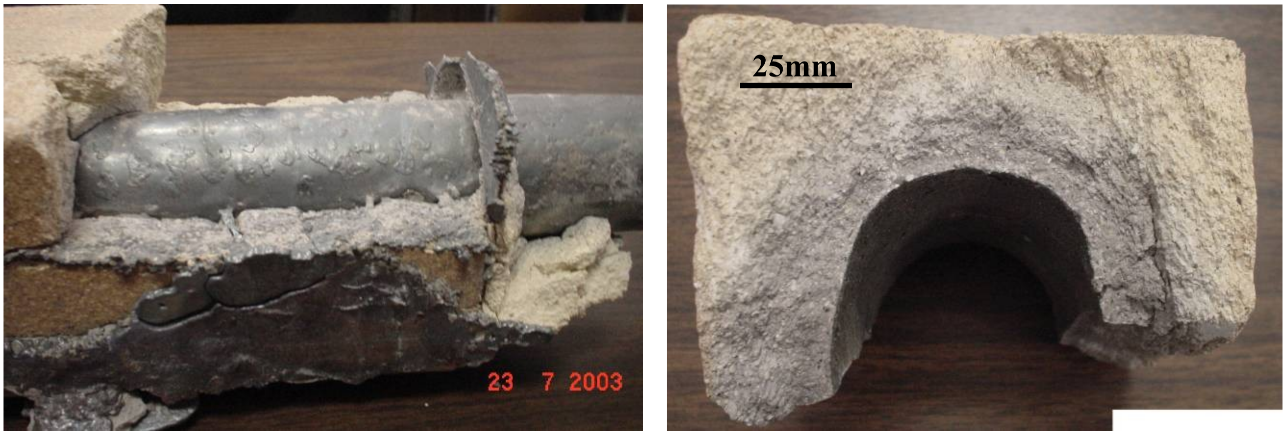

Fig.4 Used Runner Brick

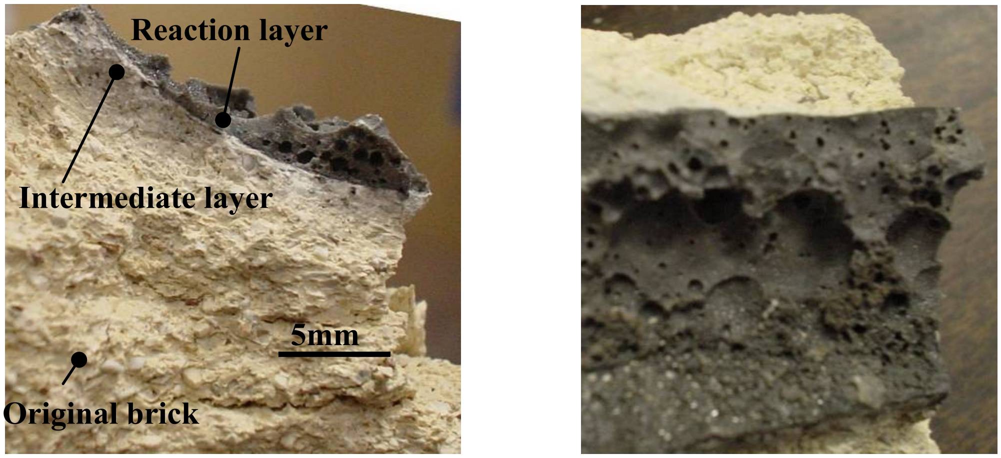

Fig.5　Runner slag

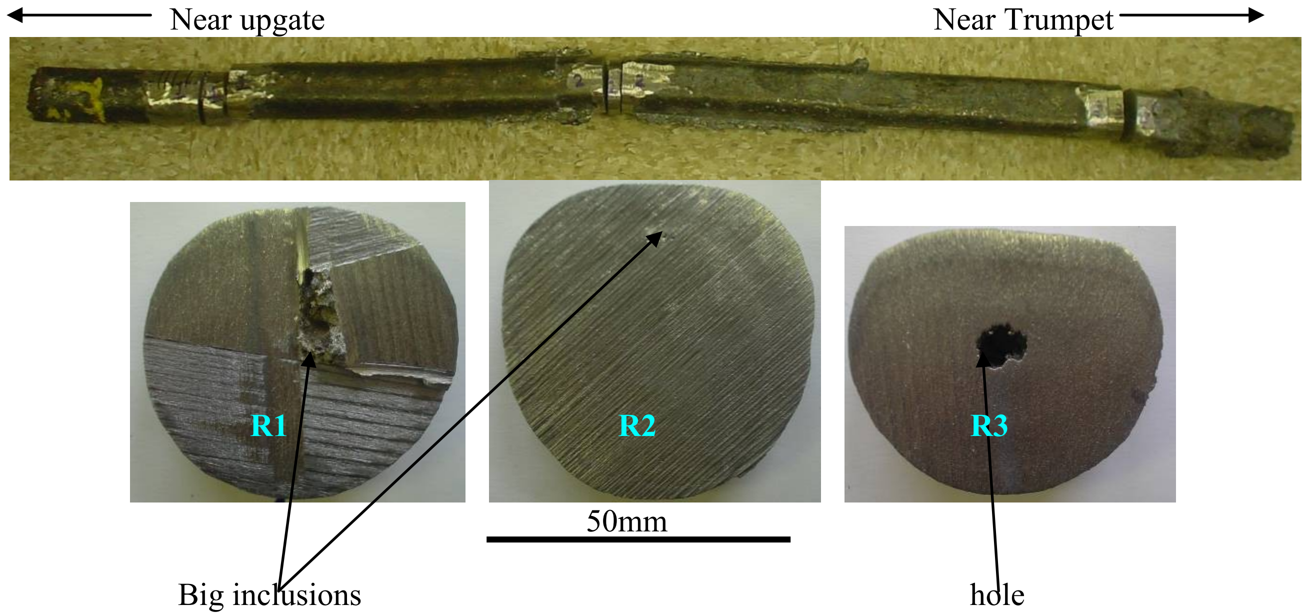

Fig.6 Runner steel samples (near upgate, runner midpoint, and near trumpet from left to right)

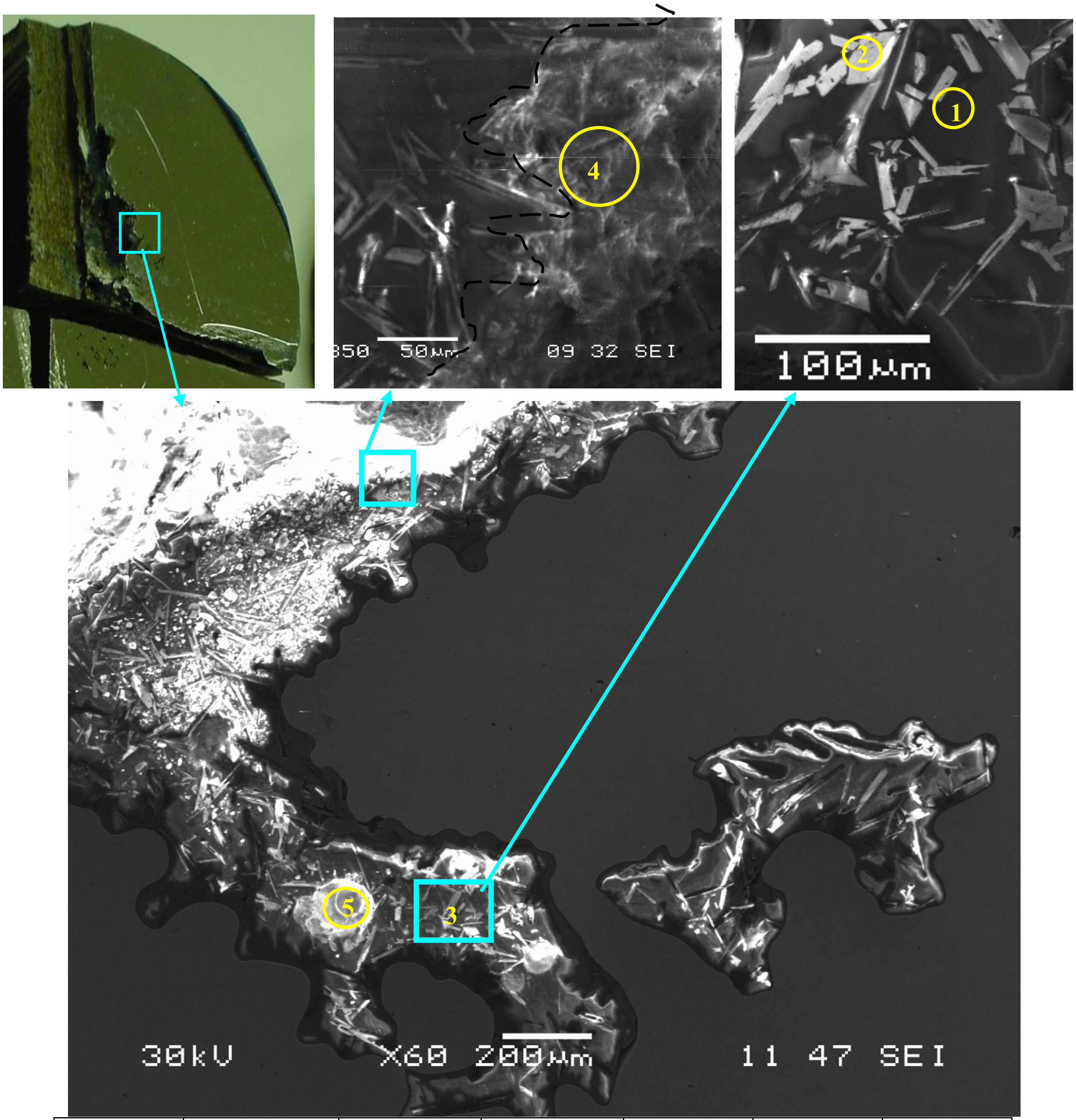

	Al_2O_3	SiO_2	MnO	K_2O	Na_2O	TiO_2
1	19.93	40.02	36.23	1.23		2.57
2	100					
3	47.16	32.75	20.09			
4	7.12	78.39	11.21		1.94	
5	3.88	82.4	10.20	1.23	1.39	

Fig.7 MnO-rich inclusions at the center of runner steel samples

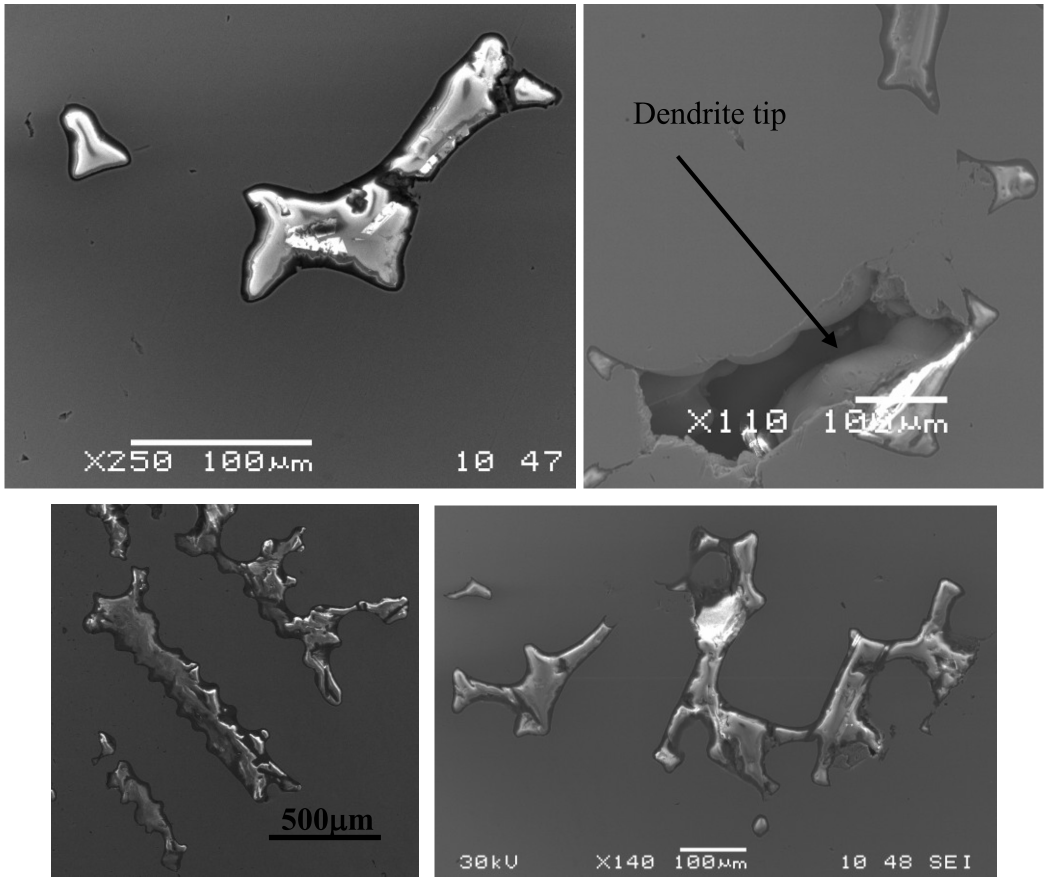

Fig.8 MnO-rich inclusions distribute along the dendritic gap

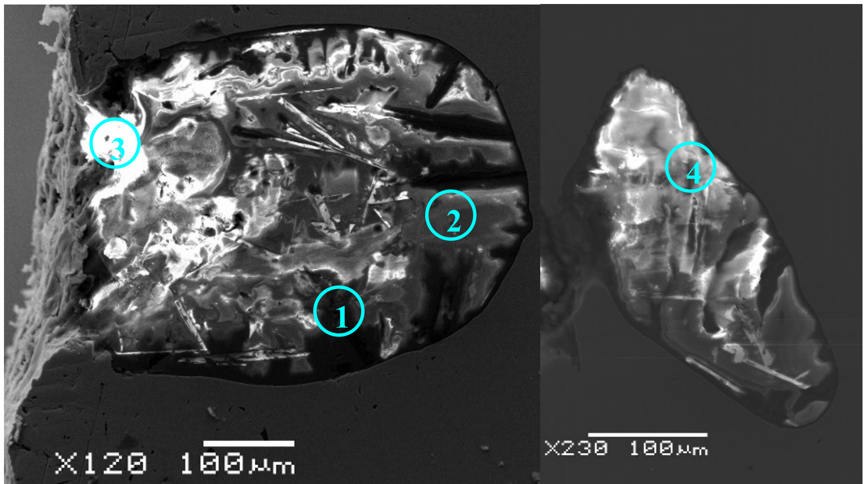

	Al_2O_3	SiO_2	MnO	K_2O	Na_2O	TiO_2
1	22.65	32.60	40.76	1.52	/	2.47
2	34.1	48.86	17.04			
3	3.11	66.80	28.28	1.31		
4	3.14	85.58	10.17		1.11	

Fig.9 MnO-rich inclusions near the edge of runner steel samples

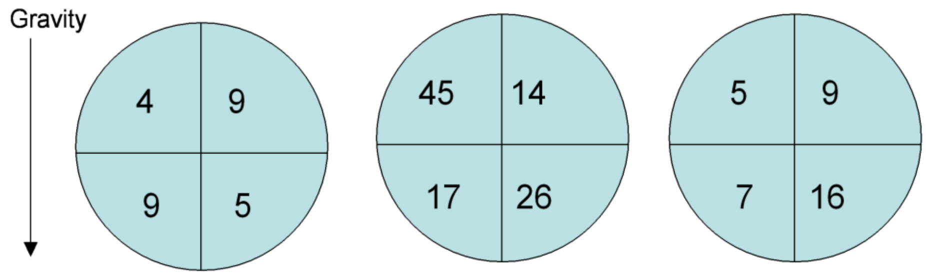

Fig.10 Inclusion distribution on runner steel samples